American Mineralogist, Volume 91, pages 127–134, 2006

High-pressure proton disorder in brucite

MAINAK MOOKHERJEE* AND LARS STIXRUDE

Department of Geological Sciences, University of Michigan, Ann Arbor, Michigan 48109, U.S.A.

ABSTRACT

In this paper we explore the structure and physical properties of brucite over a wide range of pressures with density functional theory using the variable cell-shape plane wave pseudopotential method in the local density (LDA) and generalized gradient (GGA) approximations. We probe the energetics underlying the structure and dynamics of the proton sub-lattice by performing a series of constrained and unconstrained static calculations based on an energetically stable $\sqrt{3}\times\sqrt{3}\times1$ super-cell wherein proton locations are related to the 6*i* Wyckoff sites as opposed to the ideal 2*d* site. The displacement of the hydrogen atom from the threefold axis increases with increasing pressure. This means that even in the absence of thermal energy, the protons are frustrated and would be expected to exhibit long-range disorder akin to a spin glass. To shed light on the dynamic nature of the proton hopping between the 6*i*-like sites, we determined the activation energy barrier for such jumps. We found that the energy barrier increases with compression, possibly indicating a transition from dynamic proton disorder at lower pressures to static disorder at higher pressure. We have also investigated the possibility of proton jumps across the interlayer, by determining the potential energy well along the O···O vector. We infer that proton jumps across the interlayer are either severely limited or highly cooperative since we did not find any evidence for a double well along the O···O vector. The absence of a double well along the O···O vector, the evolution of O-H···O distances with compression, and the gradual transition to a symmetric O-H···O configuration, all argue for weak hydrogen bonding in brucite.

Keywords: High-pressure study, brucite, quantum mechanical calculations, DFT, order-disorder, proton, crytal structure

INTRODUCTION

Crystallographically bound hydrogen plays an important role in the Earth's interior by modifying physical and thermodynamic properties and through hydration and dehydration reactions such as those associated with fluid release in subduction zones. Brucite $Mg(OH)_2$ serves as a model system for hydrous phases of the Earth's crust and mantle. Its simple structure provides unique insights into the nature of hydrogen bonding at elevated pressure and its influence on physical properties.

The structure of brucite prompts two fundamental questions: the location of the hydrogen atoms and the role of hydrogen bonding in stabilizing the structure. The sheets of this layered structure are composed of planes of Mg ions surrounded by planes of hydroxyl ions. Observation of the pressure-induced decrease of the hydroxyl stretching frequencies has been interpreted in terms of strengthening hydrogen bonding upon compression. On the other hand, theoretical studies have argued based on the electronic structure that hydrogen bonding is not important in brucite (Sherman 1991; Raugei et al. 1999). Our analysis of the influence of pressure on the geometry of the hydroxyl bonds supports the view that point-dipole interactions, rather than hydrogen bonding, are the primary binding agents.

The symmetry of the local environment about the ideal hydrogen position leads one to expect proton disorder. Indeed, neutron diffraction shows that the average hydrogen position does not coincide with the threefold axis at elevated pressure, but is split among three symmetrically equivalent off-axis positions (Parise et al. 1994). What is the nature of the disorder that underlies this observation? One may consider two non-exclusive possibilities: (1) dynamic disorder, in which each hydrogen hops from one to another of the three symmetrically equivalent sites with some finite time scale that is small compared with that of the experimental probe; (2) static disorder, in which each hydrogen atom is stationary, occupying for long periods of time one of the three symmetrically equivalent positions with a pattern of occupation that lacks order on a spatial scale that is small compared with that of the experimental probe. We argue that brucite undergoes two pressure-induced transitions from nearly ordered, to dominantly dynamic disorder, to dominantly static disorder.

Using density functional theory, we studied the properties of the ground state structure and the energetics underlying proton dynamics. Our investigations are complementary to previous first-principles molecular dynamics simulations at finite temperature (Raugei et al. 1999). We used static calculations to our advantage by exploring in detail pressure-induced trends in equilibrium structural parameters, by mapping out the energy surface that underlies the dynamics of proton disorder, and by exploring a much wider pressure range than previous studies. Our study further tests the ability of density functional theory to capture the relevant physics of strongly anisodesmic systems such as brucite and clays with a large range of bond strengths

* E-mail: mainak@umich.edu

from the strong hydroxyl bond to the much weaker interlayer forces (Stixrude 2003; Stixrude and Peacor 2002).

In the following section, we describe the structural model that we use to approximate proton-disordered brucite, and our computations based on density functional theory. Results include fundamental tests of the computations including comparison with the experimental equation of state, structural parameters, and explorations of the energetics of proton dynamics. We discuss our results in light of previous theoretical and experimental studies of brucite.

METHODOLOGY

Structural model

The crystal structure of brucite was first refined by Zigan and Rothbauer (1967) in space group $P\bar{3}m1$ with protons on the threefold axis corresponding to the 2*d* Wyckoff position (1/3, 2/3, *z*) (Fig. 1). Each OH vector is surrounded by three oppositely oriented hydroxyl groups of the overlying layer. Zigan and Rothbauer (1967) and subsequent studies found unusually large thermal motion of the protons (Partin et al. 1994). Neutron diffraction shows that at elevated pressure the hydrogen atoms are displaced from the fold axis. The spatially and temporally averaged hydrogen atom positions can be modeled as 1/3 occupancy of three equivalent 6*i* Wyckoff position (x, $2x$, z) with $x > 1/3$ (XGT arrangement) (Parise et al. 1994, 1998, 1999; Catti et al. 1995). An alternative arrangement with $x < 1/3$ (XLT) has also been proposed (Megaw 1973). The XGT sites minimize H····O distances. Neutron diffraction studies suggest that protons may be located at XGT sites even at ambient pressure (Desgranges et al. 1996).

To capture transitions from the conventional to the trifurcated structure in our static calculations, we adopted a model that permits an energetically favorable arrangement of deflected hydrogen bonds with the hydrogen atoms occupying 6*i*-like positions. Based on a $\sqrt{3}\times\sqrt{3}\times1$ supercell, the protons are distributed among XGT-like sites so that they form rings about the Mg atoms. This ring pattern is a compromise between the size of the unit cell (and thus computational cost) and the energetics of H-H repulsion which are frustrated on the hexagonal lattice (Fig. 2). The resulting space group is $P\bar{3}$ (a maximal subgroup of $P\bar{3}m1$), with the loss of the mirror planes as the protons are disordered spatially. The Mg atoms are located at two distinct positions, Wyckoff site 1*a* (0, 0, 0) and 2*d* (1/3, 2/3, z_{Mg}). The oxygen atoms and protons are located at general 6*g* sites with fractional coordinates (x_O, y_O, z_O) and (x_H, y_H, z_H), respectively (Table 1). Figure 2 shows the relationship between the original $P\bar{3}m1$ unit cell, a $\sqrt{3}\times\sqrt{3}\times1$ supercell, and the $P\bar{3}$ unit cell.

TABLE 1. Structure of brucite

V (Å^3)	40.20*	35.16*	41.78†	36.36†	23.34†
P (GPa)	0.4	9.3	0.3	8.4	119.1
a (Å)	3.1382(2)	3.0365(6)	3.1989	3.0887	2.6445
c (Å)	4.713(1)	4.403(2)	4.8435	4.4014	3.8516
z_{Mg}	0.000	0.000	0.0109	0.0157	0.0151
x_O	0.333	0.333	0.3321	0.3317	0.3307
			(0.3371)	(0.3407)	(0.3443)
y_O	0.666	0.666	0.3346	0.3362	0.3375
			(0.6704)	(0.6728)	(0.6761)
z_O	0.214(3)	0.232(2)	0.2200	0.2396	0.2746
x_H	0.367(4)	0.402(4)	0.3165	0.3000	0.2146
			(0.3821)	(0.4256)	(0.5408)
y_H	0.674(4)	0.804(4)	0.3493	0.3628	0.3777
			(0.7163)	(0.7628)	(0.9485)
z_H	0.412(2)	0.449(2)	0.4220	0.4525	0.4811

* Experiment (Parise et al. 1994). Space group $P\bar{3}m1$, $Z = 1$, hydrogen at Wyckoff position 6*i*.
† Theory (this study). Space group $P\bar{3}$, $Z = 3$, hydrogen at Wyckoff position 6*g*, O at position 6*g*, Mg at position 1*a* and 2*d*. In parentheses, we give the *x* and *y* coordinates referred to $P\bar{3}m1$ lattice vectors (cf. Fig. 2) to allow direct comparison with experimental values. Value reported for *a* is $1/\sqrt{3}$ the $P\bar{3}$ lattice parameter. Pressure is from GGA without thermal correction.

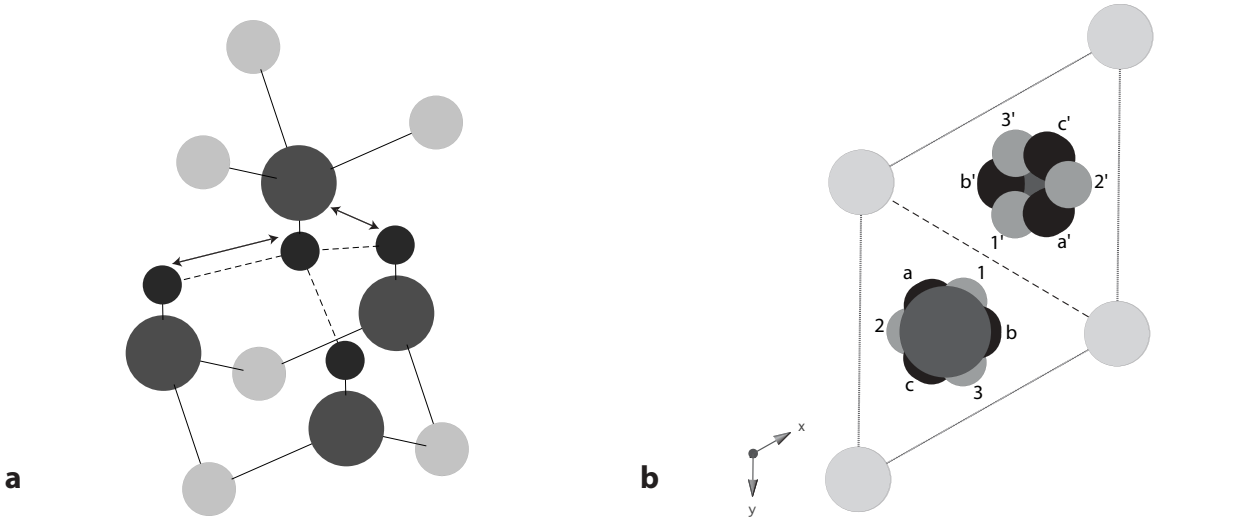

FIGURE 1. Crystal structure of brucite $Mg(OH)_2$, (**a**) perspective view of the $P\bar{3}m1$ structure showing the downward pointing proton surrounded by three upward pointing protons. The Mg atoms are denoted by light gray filled circles, the oxygen atom by dark-gray filled circles, and the proton in the 2*d* position (1/3, 2/3, z_H) by a black filled circle. The solid arrows denote the H···H interaction and point-dipole interactions; (**b**) protons shown in 6*i* Wyckoff position with fractional coordinates (x, $2x$, z). There are two classes of these positions: $x < 1/3$ (XLT) denoted by black filled circles pointing toward the Mg atoms, and $x > 1/3$ (XGT) denoted by light gray filled circles pointing toward the oxygen atoms. XGT positions are labeled 1, 2, 3 (downward pointing) and 1', 2', and 3' (upward pointing) while XLT positions are labeled a, b, c (downward pointing) and a', b', and c' (upward pointing).

We also considered the XLT arrangement of protons without the loss of mirror planes, i.e., having the same space group $P\bar{3}m1$ as the 2*d* configuration. We found that the proton relaxes back to the 2*d* positions over the entire range of pressures. The XLT arrangement is therefore unfavorable energetically and unstable mechanically in our calculations, confirming the interpretation of the neutron diffraction results by Desgranges et al. (1996) who also preferred the XGT arrangement.

We compared the energy of the $P\bar{3}$ supercell with all atoms in fully optimized positions to that of the $P\bar{3}m1$ structure with hydrogen on 2*d* positions. We also explored the energetics of hydrogen dynamics in a series of constrained calculations by systematically altering the position of one of the protons in two ways: (1) movement along the closest O-O vector across the interlayer to investigate the possibility of across-layer hopping, and (2) alteration of the azimuthal angle of one hydroxyl bond to explore the energetics of hopping among the three 6*i*-like sites (Fig. 2). These tests of the energetics of hydrogen motion, since they involve the motion of a single hydrogen atom in our $\sqrt{3}\times\sqrt{3}\times1$ supercell, break the symmetry and lower it to *P*1.

Theory

Our calculations are based on density functional theory (Kohn and Sham 1965). We investigated two widely used approximations to the exchange-correlation functional: the local density approximation (LDA) and the generalized gradient approximation (GGA) (Lundqvist and March 1987; Perdew and Wang 1986; Perdew et al. 1991). One further approximation was made, the pseudopotential approximation (Heine 1970), motivated by the argument that the core electrons participate little in bonding and structural changes. We used ultra-soft pseudopotentials (Vanderbilt 1990; Kresse et al. 1992), which limited the size of the plane wave basis set that was required to accurately represent charge density and potential.

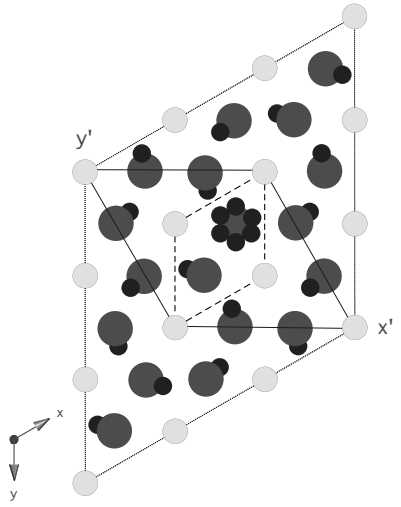

FIGURE 2. The model $P\bar{3}$ structure viewed down the c-axis with atoms shown at their equilibrium positions at a volume per formula *V*=23 Å^3. The relationship between the primitive $P\bar{3}m1$ unit cell (long-dashed lines), a $3\times3\times1$ super-cell (dotted lines) and the $P\bar{3}$ unit cell (solid lines) is indicated. The $P\bar{3}$ structure has oxygen atoms and hydrogen atoms on general sites (Wyckoff position 6*g*) and two distinct Mg sites located on the $\bar{3}$ axis at the origin (1*a*), and on the 3-fold axis without site center of symmetry (2*d*). Our strategy for exploring the energetics of azimuthal angle variation via a series of constrained calculations is illustrated schematically.

We used the Vienna ab initio simulation package (VASP) (Kresse and Hafner 1993; Kresse and Furthmüller 1996a, 1996b) to perform our calculations. We used an energy cutoff, E_{cut} = 600 eV, and a Monkhurst-Pack (Monkhurst and Pack 1976) $2\times2\times2$ *k*-point mesh and a $\sqrt{3}\times\sqrt{3}\times1$ supercell. A series of convergence tests demonstrated that these computational parameters yield energies and pressures that converged to within 0.1 *m*eV and 0.3 GPa respectively.

The equation of state and linear compressibility were analyzed using third-order Eulerian finite-strain theory (Birch 1978; Meade and Jeanloz 1990). Our calculations were static and thus neglected the influence of lattice vibrations. We estimated the effects of zero-point motion and finite temperature (300 K) by applying a semi-empirical correction to the pressure based on the Mie-Grüneisen-Debye formulation with values of the Debye temperature Θ_o = 697 K (Kieffer 1979) and Grüneisen parameter γ_o = 1.16 (Redfern and Wood 1992; Xia et al. 1998) estimated from experimental data, and the logarithmic volume derivative of γ, q = 1 (Stixrude 2003; Panero and Stixrude 2004). The thermal pressure was assumed to be isotropic: structural parameters other than the volume, such as the *c*/*a* ratio, were assumed to be functions of the volume only.

RESULTS

Energetics and EOS

We found that our model $P\bar{3}$ structure has a lower energy than that of the $P\bar{3}m1$ structure (Fig. 3). The energies of the two structures approach each other gradually on expansion, becoming indistinguishable at a volume per formula unit V = 43 Å^3.

The theoretical bulk modulus agrees well with the experimental data: both GGA and LDA values lie within the range that has been experimentally reported (Fig. 4, Table 2). The zero-pressure volume is much more sensitive to the form of the exchange-correlation functional and is in substantially poorer agreement with experiment: the theoretical volume corrected to 300 K is 7.2% larger than experiment in GGA and 6.5% smaller than experiment in LDA (Fig. 4, Table 2).

The calculated *c*/*a* ratio agrees with the experimental value to within a few percent (Fig. 5). Our calculations show strongly anisotropic compression in agreement with experiment: the *c* parameter is approximately five times more compressible than the *a* parameter at zero pressure (Table 2). The *c*/*a* ratio becomes nearly pressure independent at around 18 GPa for both the model structure and the 2*d* structure, an observation consistent with previous experimental studies (Fig. 5). Powder diffraction studies exhibited discontinuities in the *c*/*a* ratio at 6–7 GPa (Catti et al. 1995); and 10 GPa (Fei and Mao 1993). We found no such discontinuity, which may be attributed to non-hydrostatic stresses

TABLE 2. Bulk modulus (K_o), its pressure derivative (K_o'), and linear moduli (K_a, K_c) of brucite at ambient pressure

V_o (Å^3)	*c*/*a*	K_o(GPa)	K_o'	K_a(GPa)	K_c(GPa)	Method	Reference
40.88	1.516	54.3	4.7	388	75	PXD*	Fei and Mao (1993)
40.56	1.498	39.0	7.6	313	57	PND†	Catti et al. (1995)
40.85	1.516	42.0	5.7			SCXD‡	Duffy et al. (1995c)
40.8	1.516	36.7		238.1	54.6	B§	Xia et al. (1998)
40.8	1.516	39.7	6.7	263.2	51	PXD*	Xia et al. (1998)
40.2	1.502	47	4.7	277.7	138.9	PND†	Parise et al. (1994)
40.92	1.516	41.8	6.6			PXD*	Fukui et al. (2003)
41.7	1.56	43	5.7	265.55	53.19	GGA	this study
36.7	1.46	65	6.05	290	61	LDA	this study
43.8	1.58	34	5.8	225	39	$GGA^{300\ K}$	this study
38.2	1.47	53	6.2	234	45	$LDA^{300\ K}$	this study

Notes: Experimental results are at room temperature. For the theoretical results, we report both the static values and values with semi-empirical thermal correction (300 K) as discussed in the text.
* PXD = Powder X-ray diffraction.
† PND = Powder neutron diffraction.
‡ SCXD = Single-crystal X-ray diffraction.
§ B = Brillouin scattering.

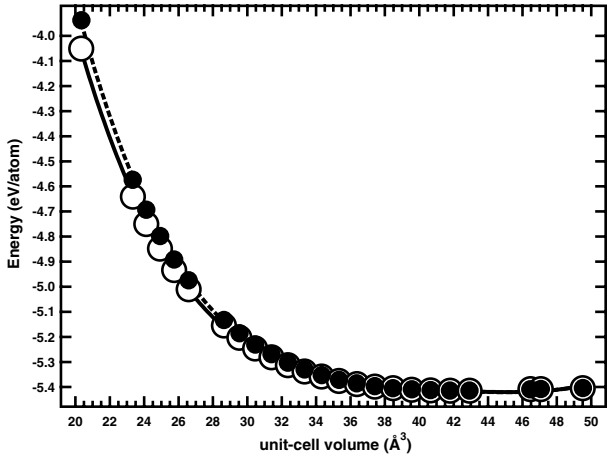

FIGURE 3. Total energy (GGA) of brucite in the $P\bar{3}$ model structure (open circles) and in the $P\bar{3}m1$ structure with hydrogen at the 2*d* positions (filled circles).

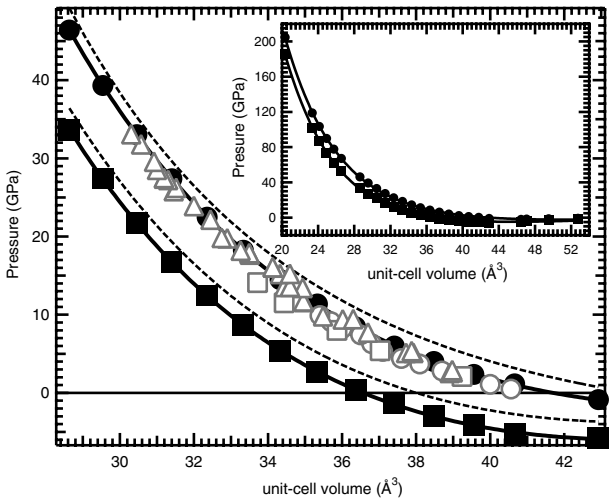

FIGURE 4. Theoretical equation of state of brucite, Filled square and solid line: LDA static; filled circle and solid line, GGA static; dashed lines: theoretical results corrected semi-empirically to room temperature (see text); open triangles, experimental data from Fei and Mao (1993); open squares, experimental data from Duffy et al. (1995c); open circles, experimental data from Catti et al. (1995). The inset shows the entire pressure range explored in this study (solid square: LDA static; solid circle: GGA static).

as confirmed by a single-crystal study (Duffy et al. 1995c). Subsequent discussions refer to both LDA and GGA results, although since both approximations show similar trends, all figures shown hereafter correspond to GGA.

The structure of the Mg-O sub-lattice remains nearly identical to that of the $P\bar{3}m1$ structure over nearly twofold compression. The atomic coordinates x_O, y_O, and z_{Mg} vary by no more than 0.02 from their values in the higher symmetry structure (Table 1).

High pressure behavior of protons

Structure. In the present study, the hydroxyl bond length r_{OH} remained almost constant with pressure, showing a very slight

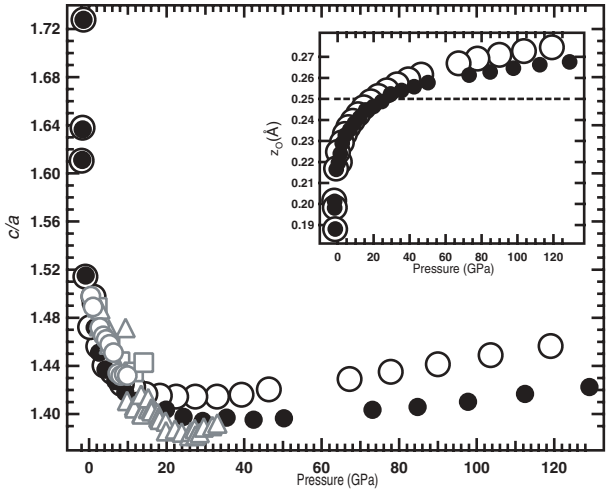

FIGURE 5. *c*/*a*-ratio vs. pressure: large open circle, GGA (300 K) for the model $P\bar{3}$ structure; filled circles, GGA (300 K) with protons at the 2*d* positions; open triangle, experimental data from Fei and Mao (1993), open squares, experimental data from Duffy et al. (1995c); open circles, experimental data from Catti et al. (1995), inset shows variation of z_O with pressure (open circle: $P\bar{3}$; filled circle: $P\bar{3}m1$).

increase, while r_{OO} and $r_{O\cdots H}$ shortened nearly linearly with compression (inset of Fig. 6). At $V = 20$ Å^3 $r_{O\cdots H}$ becomes equal to r_{OH}, producing a symmetric O-H-O arrangement. The symmetrization of the hydrogen bond is best followed by monitoring the evolution of r_{OH} as a function of r_{OO} which in turn is a function of pressure. In Figure 6 we compare r_{OH} vs. r_{OO} behavior for iceVIII, δ-AlOOH, phase-D, and various other $M(OH)_2$ phases ($M = Mg^{2+}$, Mn^{2+}, and Co^{2+}).

The inclination of the O-H vector with respect to the **c** (α_{OH}) increases upon compression from a value of 7° at the experimental zero pressure volume to 42° at $V = 20$ Å^3 (Fig. 7). We compare this inclination to that of the O···O vector, α_{OO} which is greater at all volumes studied. The inclinations α_{OH} and α_{OO} converge upon compression. The hydrogen bond angle θ, increases with compression but saturates at a value substantially less than 180° (inset Fig. 7).

The $P\bar{3}$ structure has two distinct H···H distances, which behave very differently upon compression (Fig. 8). Initially, d_{II} and d_{IV} both decrease with compression. At a volume of 36 Å^3 ($P = 8.4$ GPa), d_{IV} begins to increase with compression. The increase in d_{IV} is due to the increase in the hydroxyl inclination angle with pressure. The distance d_{II} is similar to the H···H distance in the 2*d* structure at all volumes, while d_{IV} is substantially greater at high pressure.

Energetics. We approximated the O-H···O potential well by performing a series of constrained calculations in which we moved the proton along the O···O vector. The potential well remains nearly flat across the entire pressure range of our study (Fig. 9). There is no sign of a double well structure at any pressure.

The energy barrier to proton hopping among the equivalent 6*i*-like (6*g*) sites was estimated by varying the azimuthal angle φ of a single hydrogen atom in a series of constrained calculations (Fig. 10). The energy barrier increases monotonically as

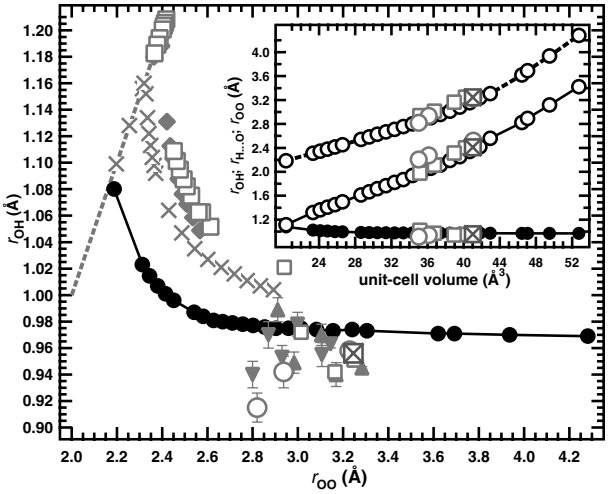

FIGURE 6. Plot of r_{OH} as a function of r_{OO}, the dashed line depicts the $r_{OO} = 2r_{OH}$ state, i.e., symmetric hydrogen bonding. The solid line with filled circles refers to $Mg(OH)_2$ using GGA; crosses refer to ice VII using GGA; large open squares and filled rhombs corresponds to theoretical study of symmetrization of hydrogen bonds in phase D and δ-AlOOH respectively (Tsuchiya et al. 2005; Panero and Stixrude 2004); open squares refer to $Mg(OD)_2$, Parise et al. (1994); open circles refers to $Mg(OH)_2$, Catti et al. (1995); square with a cross, Desgranges et al. (1996); filled downward triangles refer to β-$Co(OD)_2$, Parise et al. (1998); filled upward triangles refer to $Mn(OD)_2$, Parise et al. (1998). Inset: hydrogen bond distances vs. unit-cell volume. The data points correspond to results obtained from GGA calculations, dashed line with open circles, O···O distances; solid line with open circles, O···H distances; solid line with filled circles, O-H distances. Experimental data points included for comparisons, open squares, Parise et al. (1994), open circles, Catti et al. (1995); square with a cross, Desgranges et al. (1996).

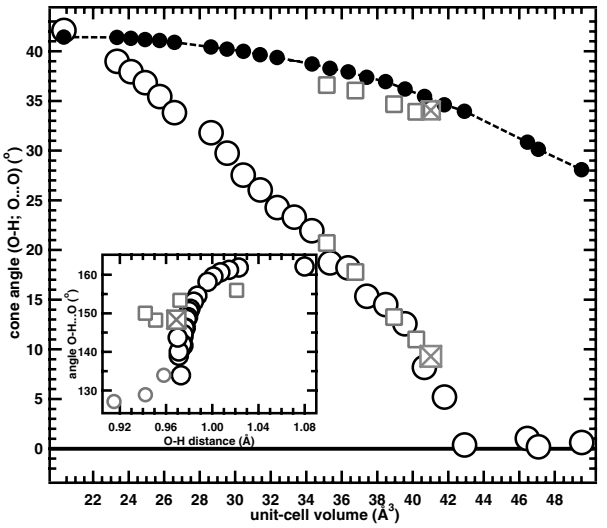

FIGURE 7. Plot of the cone angles (α_{OH} and α_{OO}) vs. unit-cell volume. The data points correspond to the results from GGA theory, open circles, O-H cone angle, dashed lines with filled circles, O-O cone angle. Experimental data points included for comparison: open squares, Parise et al. (1994), square with a cross, Desgranges et al. (1996). Inset shows O-H···O angle vs. O-H distances from GGA theory (open circles), open squares, Parise et al. (1994), open circles, Catti et al. (1995), square with a cross, Desgranges et al. (1996).

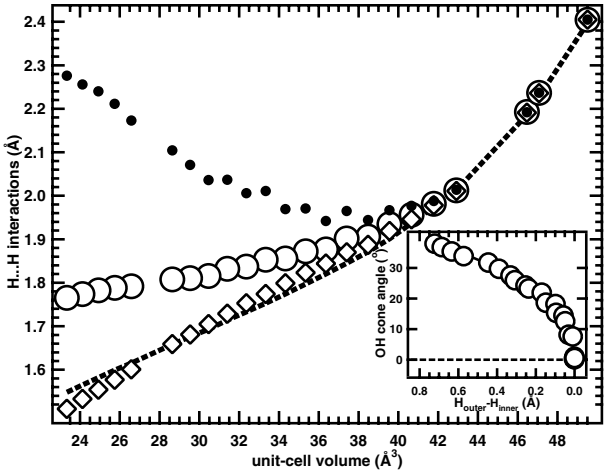

FIGURE 8. Plots of H···H distances in our model $P\bar{3}$ structure vs. unit-cell volume, open rhombs, d_{II} filled circles, d_{IV} open circles, the average H···H distance; dashed line, calculated H···H distance in the 2*d* structure. The inset shows O-H cone angle (α_{OH}) vs. difference between d_{IV} and d_{II}. At large volumes, the cone angle is 0° and $d_{II} = d_{IV}$, upon compression, the cone angle increases steeply due to point-dipole forces. Upon further compression, H···H repulsive forces overcomes the point-dipole attractive interactions and d_{IV}-d_{II} varies linearly with α_{OH}.

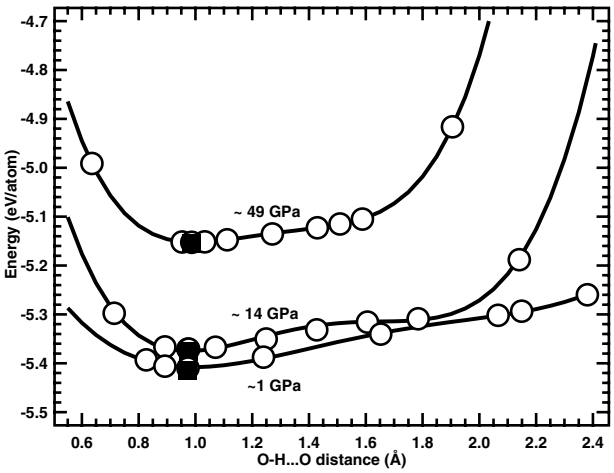

FIGURE 9. Potential well obtained by moving one proton along the O···O vector in the $P\bar{3}$ supercell. The black squares denote the fully relaxed structure. GGA results at various pressures are denoted by open circles. Lines are fits with a double-well function that are meant only to guide the eye. The poor fit at 14 GPa is due to the limitations of the fitting function and show that our first principles results do not follow a double well structure.

the lattice is compressed from less than 1 meV/atom to greater than 60 meV/atom (Fig. 11).

The energy difference between the $P\bar{3}$ structure and that of the $P\bar{3}m1$ structure with hydrogen atoms at 2*d* sites ΔE_α was compared with the activation energy barrier ΔE_φ. Both energy differences increase on compression, although ΔE_φ increases more rapidly. A plot of ΔE_α vs. α_{OH} clearly demonstrates the fact that at ambient conditions when the energy difference between

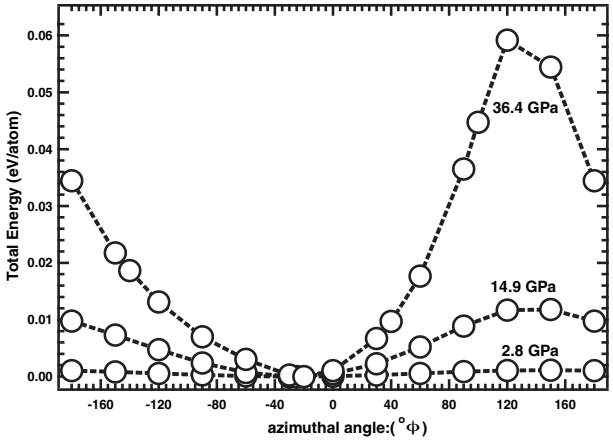

FIGURE 10. Activation energy for proton hopping shown as total energy of the model $P\bar{3}$ structure as a function of the azimuthal angle φ of one OH vector. The zero azimuthal angle is parallel to the *x* axis of the $P\bar{3}$ unit cell (Fig. 2) and corresponds to the $P\bar{3}m1$ 6*i* Wyckoff position of the protons.

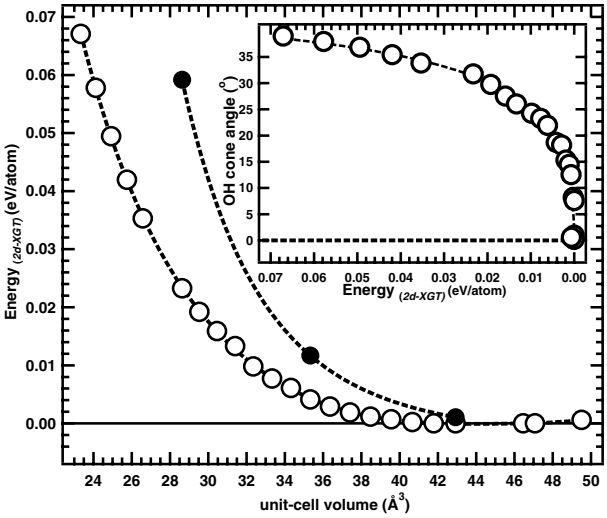

FIGURE 11. Energy difference ΔE_α (unfilled circles) between the ordered structure with protons in the 2*d* site and the model $P\bar{3}$ structure compared with the activation energy ΔE_φ (filled circles) of the proton hopping at different pressures. The inset shows O-H cone angle α_{OH} vs. ΔE_α.

the ordered (2*d*) and disordered structure is small, the proton indeed occupies the 2*d* position with zero inclination of the OH vector (Fig. 11).

DISCUSSION

Agreement between theory and experiment for many thermodynamic and structural properties including the bulk modulus, *c*/*a* and its pressure dependence, hydroxyl bond lengths, and hydroxyl deflections indicate that both GGA and LDA capture much of the relevant physics of this highly anisotropic and anisodesmic system. On the other hand, the magnitude of the discrepancy in zero-pressure volume between theory and experiment is much larger than is typical for silicates and oxides (Karki et al. 2001). Even in other very soft systems, such as talc, the disagreement between LDA and experiment is less than that in brucite (Stixrude 2003). The disagreement between theory and experiment may be due to deficiencies of LDA/GGA in systems with highly non-uniform and anisotropic charge density, or to the approximate nature of the thermal correction that we have added to our static theoretical results.

Our study demonstrates that the rapid decrease in the pressure dependence of *c*/*a* is not related to proton disordering, as suggested by Nguyen et al. (1997) for the case of $Co(OH)_2$. We found a nearly identical variation of *c*/*a* with compression whether the protons occupy the equilibrium positions in our $P\bar{3}$ model structure, or the 2*d* positions (Fig. 5). The sudden change in the character of the pressure dependence of *c*/*a* is noted in several brucite isomorphs (Parise et al. 2000) and is related to the evolution of the intra-layer and inter-layer spacings (Nagai et al. 2000). The minimum *c*/*a* ratio occurs when the oxygen coordinate z_O = 0.25, corresponding to equal inter- and intra-layer spacings. The *c*/*a* ratio increases gradually upon further compression, behavior that is seen at the high-pressure limit of some experimental studies. The slight increase in *c*/*a* is accompanied by a slight increase in z_O beyond the value of 0.25, so that the inter-layer space is actually thinner than the octahedral layer at large compression, reflecting the relative incompressibility of the octahedra.

Our results suggest that the structural model that has been used to describe experimental observations to date may not be sufficiently flexible. Diffraction data have been modeled in terms of the $P\bar{3}m1$ space group with hydrogen occupying the 6*i* position. In this position, the *x* and *y* coordinates of the hydrogen atom are not independent of each other; the hydroxyl is constrained to an azimuthal angle identical to the nearest O-O vector. In this geometry, Parise et al. (1994) have pointed out that d_{II} decreases rapidly on compression, thereby increasing H-H repulsion dramatically and destablizing the structure. Our model $P\bar{3}$ structure shows very different behavior. The azimuthal angle of the hydroxyl is not constrained and the minimum energy value differs by 30° from that of the 6*i* position. The difference in azimuthal angle means that the rate at which d_{II} decreases on compression is substantially reduced, and is no greater than the change of the H-H distance in the ideal structure with hydrogen atoms on 2*d* positions. Although it is impossible for us to model fractional occupation with our approach, this analysis indicates that our model structure will be significantly more energetically favorable than a structure in which hydrogen atoms occupy 6*i* positions at high pressure. We suggest an analysis of diffraction data in terms of more flexible models that permit variation of the azimuthal angle.

Our calculations allow us to test the physics of bonding between the weakly interacting layers in brucite: are van der Waals forces important? The most commonly used approximations to the exchange-correlation functional, and the ones that we have adopted in our study, LDA and GGA, do not capture the physics of van der Waals bonding for which electronic interactions are strongly non-local. Since van der Waals bonding is essentially absent from our calculations, the reasonable agreement that we find with experiment demonstrates that other interlayer

forces are dominant. We have obtained similar results for clays (Stixrude 2003; Stixrude and Peacor 2002). Thus clays and layered hydroxides are fundamentally different from materials such as graphite, where additional van der Waals-like forces are essential for producing a bound structure (Rydberg et al. 2003). Since we argue that hydrogen bonding is weak or absent in brucite, the dominant binding energy must be electrostatic and point-dipole in nature, i.e., oxygen anion to O-H dipole. This conclusion is consistent with the analysis of binding in brucite by Raugei et al. (1999).

The energetics of hydrogen displacement off the threefold axis is the result of two forces: (1) point-dipole interaction, an attractive force, and (2) H···H interaction, a repulsive force. Our results suggest that at low pressure, the point-dipole interaction is the most important factor: the hydroxyl group is attracted electrostatically to the oxygen atom in the next layer, causing it to deviate from the threefold axis. Upon compression, the cone angle first deviates from zero at a volume ($V = 43$ Å^3) where H-H repulsion is apparently still weak as indicated by the large H-H distances and their rapid decrease with compression. At high pressures, H-H repulsion appears to dominate the evolution of the cone angle as indicated by the increase of d_{IV} with compression for volumes less than $V = 36$ Å^3.

This picture is consistent with observations of hydroxyl deflection in other $M(OH)_2$ isomorphs. The different behavior among these compounds can be rationalized in terms of cation size. Increasing cation size tends to expand the basal plane, and thus α_{OO}. Larger values of α_{OO} will lead, through the point-dipole interaction, to larger H deflection. Thus, portlandite $Ca(OH)_2$, with a larger cation than brucite, has a larger value of α_{OH} at ambient pressure (Desgranges et al. 1996). We might expect stronger signs of disorder in compounds with larger cations for two reasons. First, the larger deflection would amplify signals of disorder such as the width of vibrational lines. Secondly, compounds with larger cations will tend to have larger H-H distances, so that activation energy barriers to hopping among the threefold sites would be diminished in magnitude and would grow less rapidly with pressure. Thus the width of the OH vibrational mode grows rapidly with pressure in portlandite, less rapidly in $Co(OH)_2$ and least rapidly in brucite, a trend consistent with variation in cation size (Kruger et al. 1989; Nguyen et al. 1997; Sheih and Duffy 2002).

The anhydrous sub-lattice of portlandite amorphizes at 11 GPa for reasons that are not known (Meade and Jeanloz 1990). In contrast, brucite shows no evidence of pressure-induced amorphization of the Mg-O sublattice, which remains crystalline to pressures of 30 GPa (Kruger et al. 1989; Duffy et al. 1995a, 1995b). Our study confirms the experimental observations: although our model $P\bar{3}$ structure places the Mg atom at 2*d* and the O atom at 6*g* site, their deviation from ideal positions is small (Table 1). This demonstrates that proton deflection can co-exist with crystalline order in the Mg-O sub-lattice.

The onset and subsequent increase of hydroxyl deflection with compression suggests a transition from ordered to dynamically disordered states. At large volumes, where the equilibrium deflection is small compared with thermal vibrations, the proton may occupy the 2*d* site with greatest probability. As the underlying ground state deflection becomes larger than that of the thermal vibrations, H will deviate from the 2*d* site. Occupation of sites off the threefold axis entails energetic frustration: it is not possible to construct an ordered structure in which all H-H distances attain their maximum (e.g., 1-1') values. Disorder then is an inevitable consequence of threefold site occupation. The disorder is likely dynamic at low pressure, as suggested by the small magnitude of the energy barrier to hopping among threefold sites. The barrier is only 1 meV/atom at 2.8 GPa, which is much less than kT (0.025 eV) at $T = 300$ K where k is the Boltzmann constant Each proton will hop freely among three positions about the threefold axis, since the activation energy barrier to these transitions is small. This picture is consistent with the classical molecular dynamics simulations of Raugei et al. (1999), which extended to relatively modest pressures of 14 GPa. We note, however, that a complete understanding of the dynamics of the proton would have to account for its quantum nature.

The growth of the activation energy barrier to proton hopping with compression suggests a second transition, from a dynamically disordered, to a statically disordered state. As the activation barrier grows, the protons will increasingly tend to occupy only one of the threefold sites. The spatial average of such a configuration would be very similar to that of our $P\bar{3}$ structure.

Based on characteristics of the charge density, Raugei et al. (1999) argued that hydrogen bonding was not important in brucite over the pressure range of their study (<14 GPa). Sherman (1991) suggested that hydrogen bonding could become more important at large compressions as the Mg-O bond becomes more covalent, although the 2*d* structure was assumed in these calculations. The results of our study argue against hydrogen bonding in brucite based on the following results: (1) The evolution of r_{OH} and r_{OO} with pressure. r_{OH} changes little with increasing pressure and the variation of r_{OH} with r_{OO} is nearly zero until very close to symmetrization. Symmetrization occurs at a pressure well beyond the stability field. Such behavior contrasts with the strongly non-linear behavior in ice (Benoit et al. 1998), δ-AlOOH (Panero and Stixrude 2004), and phase D (Tsuchiya et al. 2005) as the conditions of symmetric hydrogen bonding are approached. (2) We find no evidence of a double well structure of the hydrogen potential well at any pressure. The lack of a double well also has important implications for the suggestion that interlayer hopping takes place in brucite (Shinoda and Aikawa 1998; Shinoda et al. 2002). Our results indicate that if such motions occur, they must be limited or highly cooperative.

We conclude that hydrous minerals, such as brucite, provide a good test of the density functional theory. We find that the local density (LDA) and generalized gradient (GGA) approximations reproduce many features of the experimentally observed structure and equation of state to within a few percent. Theory allows us to explore portions of the equations of state that have not yet been examined experimentally.

The proton disorder is energetically favored, as observed from the lower energy of our $P\bar{3}$ model structure as compared with the $P\bar{3}m1$ structure, over a wide pressure range. We find that protons are more stable in XGT-like than in XLT-like positions. Proton disorder is likely to be dynamic at lower pressures. The activation energy for the reorientation of protons among the energetically equivalent sites increases with pressure indicating that the disorder may become increasingly static with compression. Hydrogen

bonding appears to be energetically unimportant in brucite as revealed by the variation of the structure with compression.

ACKNOWLEDGMENT

The authors thank two anonymous reviewers whose constructive criticism improved the clarity of the article. This work was supported by the National Science Foundation under grants EAR-044227 and EAR-044863.

REFERENCES CITED

Benoit, M., Marx, D., and Parrinello, M. (1998) Tunnelling and zero-point motion in high-pressure ice. Nature, 392, 258–261.

Birch, F. (1978) Finite strain isotherm and velocities for single-crystal and polycrystalline NaCl at high pressures and 300 K. Journal of Geophysical Research, 83, 1257–1267.

Catti, M., Ferraris, G., Hull, S., and Pavese, A. (1995) Static compression and H disorder in brucite, $Mg(OH)_2$, to 11 GPa: a powder neutron diffraction study. Physics and Chemistry of Minerals, 22, 220–206.

Desgranges, L., Calvarin, G., and Chevrier, G. (1996) Interlayer interactions in $M(OH)_2$: A neutron diffraction study of $Mg(OH)_2$. Acta Crystallographica, B52, 82–86.

Duffy, T.S., Meade, C., Fei, Y., Mao, H.K., and Hemley, R. (1995a) High-pressure phase transition in brucite, $Mg(OH)_2$. American Mineralogist, 80, 222–230.

Duffy, T.S., Hemley, R.J., and Mao, H.K. (1995b) Structure and bonding in hydrous minerals at high pressure: Raman microscopy of alkaline earth hydroxides. In K.A. Farley, Ed., Volatiles in the Earth and Solar System, p. 211–220. American Institute of Physics, Woodbury, New York.

Duffy, T.S., Shu, J., Mao, H.K., and Hemley, R. (1995c) Single-crystal X-ray diffraction of brucite to 14 GPa. Physics and Chemistry of Minerals, 22, 277–281.

Fei, Y. and Mao, H.K. (1993) Static compression of $Mg(OH)_2$ to 78 GPa at high temperature and constraints on the equation of state of fluid H_2O. Journal of Geophysical Research, 98, 11875–11884.

Fukui, H., Ohtaka, O., Suzuki, T., and Funakoshi, K. (2003) Thermal expansion of $Mg(OH)_2$ brucite under high pressure and pressure dependence of entropy. Physics and Chemistry of Minerals, 30, 511–516.

Heine, V. (1970) The pseudopotential concept. Solid State Physics, 24, 1–37.

Karki, B.B., Stixrude, L., and Wentzcovitch, R.M. (2001) Elastic properties of major materials of Earth's mantle from first principles. Reviews of Geophysics, 39, 507–534.

Kieffer, S.W. (1979) Thermodynamics and lattice vibration of minerals: 3. Lattice dynamics of an approximation for minerals with application to simple substances and framework silicates. Reviews of Geophysics and Space Physics, 17, 35–59.

Kohn, W., and Sham, L.J. (1965) Self-consistent equations including exchange and correlation effects. Physical Review A, 140, 1133–1138.

Kresse, G. and Furthmüller, J. (1996a) Efficiency of ab-initio total energy calculations for metals and semiconductors. Computational Material Science, 6, 15–50.

——— (1996b) Efficient iterative schemes for ab-initio total energy calculations using a plane-wave basis set. Physical Review B, 54,11,169–11,186.

Kresse, G. and Hafner, J. (1993) Ab initio molecular-dynamics for liquid metals. Physical Review B, 47, 558–561.

Kresse, G., Hafner, J., and Needs, R.J. (1992) Optimized norm-conserving pseudopotentials. Journal of Physics Condensed Matter, 4, 7451–7468.

Kruger, M.B., Williams, Q., and Jeanloz, R. (1989) Vibrational spectra of $Mg(OH)_2$ and $Ca(OH)_2$ under pressure. Journal of Chemical Physics, 91, 5910–5915.

Lundqvist, S. and March, N. H. (1987) Theory of the Inhomogenous Electron Gas. Plenum Press, New York.

Meade, C. and Jeanloz, R. (1990) Static compression of $Ca(OH)_2$ at room temperature: observation of amorphization and equation of state measurements to 10.7 GPa. Geophysics Research Letters, 17, 1157–1160.

Megaw, H.D. (1973) Crystal Structures: A Working Approach. W.B. Sanders Company, Philadelphia.

Monkhurst, H.J. and Pack, J.D. (1976) Special points for Brillouin-zone integration. Physical Review B, 13, 5188–5192.

Nagai, T., Hattori, T., and Yamanaka, T. (2000) Compression mechanism of brucite: An investigation by structural refinement under pressure. American Mineralogist, 85, 760–764.

Nguyen, J.H., Kruger, M.B., and Jeanloz, R. (1997) Evidence for "partial" (sublattice) amorphization in $Co(OH)_2$. Physical Review Letters, 78, 1936–1939.

Panero, W. and Stixrude, L.P. (2004) Hydrogen incorporation in stishovite at high pressure and symmetric hydrogen bonding in δ-AlOOH. Earth and Planetary Science Letters, 221, 421–431.

Parise, J.B., Leinenweber, K., Weidner, D.J., and Tan, K. (1994) Pressure induced bonding: Neutron diffraction study of brucite, $Mg(OD)_2$, to 9.3 GPa. American Mineralogist, 79, 193–196.

Parise, J.B., Theroux, B., Li, R., Loveday, J.S., Marshall, W.G., and Koltz, S. (1998) Pressure dependence of hydrogen bonding in metal deuteroxides: a neutron powder diffraction study of $Mn(OD)_2$ and β-$Co(OD)_2$. Physics and Chemistry of Minerals, 25, 130–137.

Parise, J.B., Loveday, J.S., Nelmes, R.J., and Kagi, H. (1999) Hydrogen repulsion "transition" in $Co(OD)_2$ at high pressure? Physical Review Letters, 83, 2, 328–331.

Parise, J.B., Kagi, H., Loveday, J.S., Nelmes, R.J., and Marshall, W.G. (2000) H···H interactions and order-disorder at high pressure in layered hydroxide and dense hydrous phases. In H. Aoki, Ed., Physics Meets Mineralogy, p. 308–322. Cambridge University Press.

Partin, D.E., O'Keeffe, M., and von Dreele, R.B. (1994) Crystal structure and profile fitting of $Mg(OD)_2$ by time-of-flight neutron diffraction. Journal of Applied Crystallography, 27, 581–584.

Perdew, J.P. and Wang, Y. (1986) Accurate and simple density functional for the electronic exchange energy: Generalized gradient approximation. Physical Review B, 33, 8800–8802.

Perdew, J.P., Chevary, J.A., Vosko, S.H., Jackson, K.A., Pederson, M.R., Singh, D.J., and Fiolhais, C. (1991) Atoms, molecules, solids, and surfaces: Applications of the generalized gradient approximation for exchange and correlation. Physical Review B, 46, 6671–6687.

Raugei, S., Silvestrelli, P.L., and Parrinello, M. (1999) Pressure-induced frustration and disorder in $Mg(OH)_2$ and $Ca(OH)_2$. Physical Review Letters, 83, 2222–2225.

Redfern, S.A.T. and Wood, B.J. (1992) Thermal expansion of brucite $Mg(OH)_2$. American Mineralogist, 77, 1129–1132.

Rydberg, H., Dion, M., Jacobson, N., Schröder, E., Hyldgaard, P., Simak, S.I., Langreth, D.C., and Lundqvist, B.I. (2003) Van der Waals density functional for layered structures. Physical Review Letters, 91, 126402:1- 4.

Sherman, D.M. (1991) Hartree-Fock band structure, equation of state and pressure induced hydrogen bonding in brucite, $Mg(OH)_2$. American Mineralogist, 76, 1769–1772.

Shieh, S.R. and Duffy, T.S. (2002) Raman spectroscopy of $Co(OH)_2$ at high pressure: Implication for amorphisation and hydrogen repulsion. Physical Review B, 66, 134301:1–8.

Shinoda, K. and Aikawa, N. (1998) Interlayer proton transfer in brucite under pressure by polarized IR spectroscopy to 5.3 GPa. Physics and Chemistry of Minerals, 25, 197–202.

Shinoda, K., Yamakata, M., Nanba, T., Kimura, H., Moriwaki, T., Kondo, Y., Kawamoto, T., Niimi, N., Miyoshi, N., and Aikawa, N. (2002) High-pressure phase transition and behavior of protons in brucite $Mg(OH)_2$: a high-pressure-temperature study using IR synchrotron radiation. Physics and Chemistry of Minerals, 29, 396–402.

Stixrude, L. (2003) Talc under tension and compression: Spinodal instability, elasticity, and structure. Journal of Geophysical Research, 107, ECV2, 1–10.

Stixrude, L. and Peacor, D. (2002) First principles study of illite-smectite and implications for clay mineral systems. Nature, 420, 165–168.

Tsuchiya, J., Tsuchiya, T., and Tsuneyuki, S. (2005) First-principles study of hydrogen bond symmetrization of phase D under high pressure. American Mineralogist, 90, 44–49.

Vanderbilt, D. (1990) Soft self-consistent pseudopotentials in a generalized eigenvalue formalism. Physical Review B, 41, 7892–7895.

Xia, X., Weidner, D.J., and Zhao, H. (1998) Equation of state of brucite: single-crystal brillouin spectroscopy study and polycrystalline pressure-volume-temperature measurement. American Mineralogist, 83, 68–74.

Zigan, F. and Rothbauer, R. (1967) Neutronenbeugungsmessungen am Brucit. Neues Jahrbuch Mineralogie Montashefte, 137–143.

MANUSCRIPT RECEIVED DECEMBER 24, 2004
MANUSCRIPT ACCEPTED JUNE 1, 2005
MANUSCRIPT HANDLED BY DAN SHIM